Anomalous Josephson current in quantum anomalous Hall insulator-based superconducting junctions with a domain wall structure*

Qing Yan(闫青)[1,2], Yan-Feng Zhou(周彦峰)[3], and Qing-Feng Sun(孙庆丰)[1,2,4,†]

[1] International Center for Quantum Materials, School of Physics, Peking University, Beijing 100871, China
[2] Collaborative Innovation Center of Quantum Matter, Beijing 100871, China
[3] Department of Physics, University of Texas at Dallas, Richardson, Texas 75080, USA
[4] CAS Center for Excellence in Topological Quantum Computation, University of Chinese Academy of Sciences, Beijing 100190, China

(Received 8 May 2020; revised manuscript received 20 June 2020; accepted manuscript online 3 July 2020)

We theoretically study the Josephson effect in a quantum anomalous Hall insulator (QAHI) nanoribbon with a domain wall structure and covered by the superconductor. The anomalous Josephson current, the nonzero supercurrent at the zero superconducting phase difference, appears with the nonzero magnetization and the suitable azimuth angle of the domain wall. Dependent on the configuration of the domain wall, the anomalous current peaks in the Bloch type but disappears in the Néel type because the y-component of magnetization is necessary to break symmetry to arouse the anomalous current. The phase shift of the anomalous current is tunable by the magnetization, the azimuth angle, or the thickness of the domain wall. By introducing a bare QAHI region in the middle of the junction which is not covered by the superconductor, the anomalous Josephson effect is enhanced such that the phase shift can exceed π. Thus, a continuous change between 0 and π junctions is realized via regulating the configuration of the domain wall or the magnetization strength. As long as an s-wave superconductor is placed on the top of the QAHI with a domain wall structure, this proposal can be experimentally fabricated and useful for the phase battery or superconducting quantum bit.

Keywords: anomalous Josephson current, quantum anomalous Hall insulator, domain wall, Josephson junction

PACS: 74.45.+c, 75.60.Ch, 73.23.–b **DOI:** 10.1088/1674-1056/aba272

1. Introduction

Since theoretically proposed and experimentally confirmed, Josephson junctions[1,2] serve as an indispensable device in the research area of superconducting electronics.[3,4] Initially, the zero Josephson junction carries supercurrent I with no bias voltage, the so-called dc Josephson current, obeying the formula $I = I_c \sin\varphi$ with φ the superconducting phase difference[5] between two superconducting electrodes. When a ferromagnetic middle layer with large exchanging interactions is inserted between superconducting electrodes, the π junction forms with $I = I_c \sin(\varphi + \pi)$.[6–11] In addition, the anomalous Josephson junction can carry supercurrent even if there is no superconducting phase difference between two leads, that is, $I = I_c \sin(\varphi + \delta)$, also named as the δ junction.[12–15] This anomalous junction could not only be a natural phase shifter or a phase battery in the superconducting circuits but also be crucial for the superconducting quantum computation.[16,17]

After the first proposal of the anomalous Josephson current in the quantum wire[12,18–20] and Luttinger liquid[13] sandwiched between two s-wave superconducting electrodes, theoretical researches find the possibility of the anomalous current in the systems of quantum dots,[21–23] quantum point contacts,[15] two-dimensional electron gas,[24] quantum Hall family,[25,26] as well as ferromagnets.[17,27–30] Although the anomalous Josephson current is suggested in various systems or devices, it is still difficult to experimentally observe the anomalous current. Besides the external Zeeman field or the internal exchange field of a ferromagnet, other ingredients are necessary to break the symmetry that protects $I(\varphi) = -I(-\varphi)$ in the superconducting heterostructures, such as the spin–orbit coupling,[14,15] the spin-fliper,[17] the spin-filtering barrier,[30] or a quasiparticle injection tuned by the voltage.[29] In fact, the anomalous Josephson junction is realized merely in nanowire quantum dots[16] and topological insulators[31] in contact with normal s-wave superconducting electrodes. More experiments, simple and easy to perform, are still lacking.

Topological insulators have aroused huge interests with extraordinary properties due to the non-trivial topology coming from the strong spin–orbit coupling.[32] Combining topology and magnetism leads to the formation of magnetic topological insulators.[33–36] Since the magnetic doping breaks the time-reversal symmetry, lots of novel phenomena emerge, in-

*Project supported by the National Key R&D Program of China (Grant No. 2017YFA0303301), the National Natural Science Foundation of China (Grant Nos. 11921005 and 11574007), the Strategic Priority Research Program of Chinese Academy of Sciences (Grant No. XDB28000000), and Beijing Municipal Science & Technology Commission, China (Grant No. Z191100007219013).

†Corresponding author. E-mail: sunqf@pku.edu.cn

cluding the quantum anomalous Hall effect,[37,38] the topological magnetoelectric effect,[39] and the topological axion state.[40,41] In experiments, quantum anomalous Hall insulators (QAHIs) are successfully fabricated in Cr-doped $(Bi,Sb)_2Te_3$ films,[37,38,42] V-doped $(Bi,Sb)_2Te_3$ films,[43,44] and the intrinsic $MnBi_2Te_4$ films.[45–47] Without the external magnetic field, the precise quantized Hall conductance plateaus are observed, which confirms the chiral edge state classified by the Chern number $\mathcal{C}=1$ and paves way for the dissipationless spintronic devices.

Magnetic domain walls are the continuous transition region between magnetized domains with different magnetization directions.[48–51] Configurations of magnetic domain walls are the result of the competition of the exchange interaction, magnetic anisotropy, and dipolar interaction to minimize the total energy.[52] The Néel type and the Bloch type are two kinds of energy favorable walls, of which magnetization direction rotates perpendicularly or in parallel to domain walls.[53,54] In 2017, Yasuda *et al.*[55] successfully fabricated a magnetic domain wall in the QAHI with the tip of the magnetic force microscope and proved the transport properties of chiral edge conduction. Recall that QAHIs can be turned into superconductors due to the proximity effect with different superconducting phases marked by Chern number $\mathcal{N}=0$, $\mathcal{N}=1$, and $\mathcal{N}=2$.[56–60] Based on this precursory experiment, we propose that if an s-wave superconductor is placed on the top of the QAHI with domain walls, a QAHI-based Josephson junction forms, as shown in Fig. 1(a). Fulfilled with the superconducting pairing, the spin–orbit coupling, as well as the ferromagnetic exchanging interaction, this junction should be a good candidate for the anomalous Josephson current.

In this paper, we construct a QAHI-based Josephson junction with a domain wall structure as shown in Fig. 1(a). The magnetization direction in the domain wall gradually changes from $+z$-direction to $-z$-direction along x-direction and the configuration of this domain wall is labeled by an azimuth angle. We are interested in the anomalous Josephson effect in these aspects: (i) whether the anomalous Josephson current exists in the setup device; (ii) where the anomalous current origins and how the configuration of a domain wall structure takes effect; (iii) how to regulate the phase shift of the anomalous Josephson current and how to realize the continuous transition from the 0 junction to the π junction.

We take up the nonequilibrium Green's function to calculate the current-phase relation and find the anomalous Josephson current in the case of the nonzero magnetization as well as the nonzero azimuth angle. Based on symmetry analysis, when the M_y component of the magnetization in domain wall is zero, the QAHI-based Josephson junction system is protected by the $\sigma_y R_y \mathcal{T}$ symmetry with R_y spatial inversion operation, σ_y spin rotation operation, and $\mathcal{T}$ time-reversal operation, leading to a normal Josephson current. On the other hand, the nonzero M_y component for the domain wall configuration with a nonzero azimuth angle breaks the $\sigma_y R_y \mathcal{T}$ symmetry and results in the anomalous Josephson current. We figure out the phase shift via a Fourier transform of the current-phase relation and find that the phase shift shows a standard sinusoidal relation to the azimuth angle. We also analyze the effect of system parameters on the phase shift as well as the amplitude of supercurrent. When the azimuth angle is equal to $\pi/2$ (i.e. for the Bloch-type domain wall), the phase shift reaches its maximum value. Increasing the magnetization and thickness of the domain wall can strengthen the phase shift. The growth of junction width hardly affects the phase shift but clearly enlarges the amount of supercurrent. In addition, the anomalous Josephson current has similar behavior for the $\mathcal{N}=0$, $\mathcal{N}=1$ and $\mathcal{N}=2$ superconducting phases. Moreover, we consider another structure of the Josephson junction containing a bare QAHI region in the center of two superconductors. Bringing in the QAHI layers means decreasing the direct tunneling of the Cooper pair, and then increasing the effective magnetization and facilitating the phase shift, so the phase shift can continuously be tuned from zero to π via increasing the magnetization.

The rest of this paper is organized as follows. Section 2 describes the device consisting of the QAHI-based Josephson junction with a domain wall, the Hamiltonian, and the transport method adopted to calculate the Josephson supercurrent. Section 3 shows the appearance of the anomalous current and how the azimuth angle of the domain wall affects. Section 4 gives the symmetry analysis to explain why the anomalous current occurs. The effect of system parameters on the phase shift of the anomalous current is studied in Section 5. Section 6 studies the QAHI-based Josephson junction with inserted QAHI layers. Finally, conclusion is presented in Section 7.

2. Model and method

To describe the device consisting of the QAHI-based Josephson junction with a domain wall as shown in Fig. 1(a), we take up an eight-band Hamiltonian evolving from a four-band QAHI Hamiltonian,[37] which includes the spin–orbit interaction together with the exchanging interaction induced by magnetic doping. Explicitly, we write down the Hamiltonian of the QAHI nanoribbon with a domain wall, $H_{\rm QAHI}=\sum_{\boldsymbol{p}}\Psi_{\boldsymbol{p}}^{\dagger}H_{\rm QAHI}(\boldsymbol{p})\Psi_{\boldsymbol{p}}$, with[37]

$$H_{\rm QAHI}(\boldsymbol{p})=v_{\rm F}p_y\tau_z\sigma_x-v_{\rm F}p_x\tau_z\sigma_y+m(\boldsymbol{p})\tau_x\sigma_0+\boldsymbol{M}\cdot\boldsymbol{\sigma},\quad(1)$$

where the momentum operator $\boldsymbol{p}=(p_x,p_y)=(-\mathrm{i}\partial/\partial x,-\mathrm{i}\partial/\partial y)$ and $\Psi_{\boldsymbol{p}}=[\psi_{\boldsymbol{p},\mathrm{t}\uparrow},\psi_{\boldsymbol{p},\mathrm{t}\downarrow},\psi_{\boldsymbol{p},\mathrm{b}\uparrow},\psi_{\boldsymbol{p},\mathrm{b}\downarrow}]^{\mathrm{T}}$ with the annihilation operators $\psi_{\boldsymbol{p},\mathrm{t}\uparrow/\downarrow}$ and $\psi_{\boldsymbol{p},\mathrm{b}\uparrow/\downarrow}$ for the top and bottom layers and the up and down spins. Here $\sigma_{x,y,z}$ and

$\tau_{x,y,z}$ are Pauli matrices in the basis of spins (up and down) and layers (top and bottom), respectively, and σ_0 is a 2×2 identity matrix. The term $m(\boldsymbol{p}) = m_0 - m_1(p_x^2 + p_y^2)$ describes the coupling between the top and bottom layers, and from now on, we set $m_0 = -0.1 < 0$ such that this Hamiltonian presents the QAH phase rather than the normal insulating phase.[61]

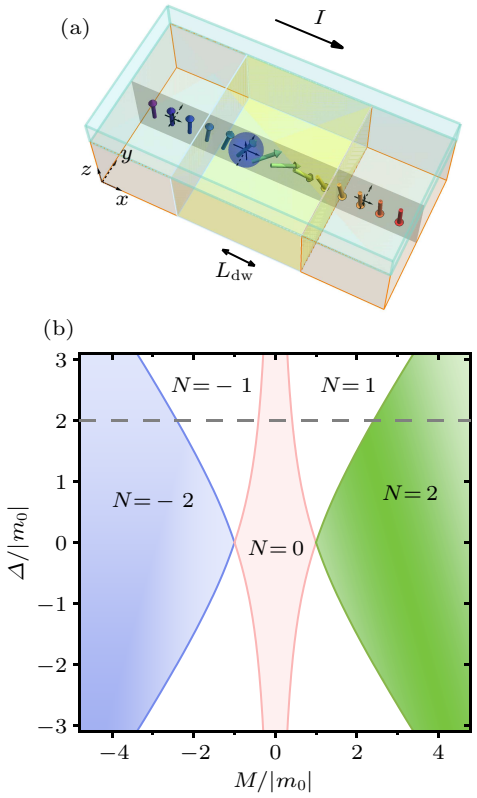

Fig. 1. (a) Schematic diagram for the QAHI-based Josephson junction: the bottom base is a QAHI nanoribbon with a domain wall structure and the top is an s-wave superconductor. The domain wall centers at the $x = 0$. The magnetization directions point to the $+z$ ($-z$) direction while the $x \ll 0$ ($x \gg 0$), but it gradually rotates from the $+z$-direction to the $-z$-direction near $x = 0$. The magnetic orientation is homogeneous along the y direction. Note: the illustration is not drawn to scale; in practice, the thickness of a domain wall $L_{\rm dw}$ is much smaller than the size of junction. (b) Phase diagram of superconductors with uniform magnetization as functions of the induced superconducting gap and magnetization. In our calculation, since $m_0 = -0.1$ and $\Delta = 0.2$, increasing magnetization from $M = 0.05$ to $M = 0.2$ to $M = 0.35$ transits the phase from $\mathcal{N} = 0$ to $\mathcal{N} = 1$ to $\mathcal{N} = 2$.

The structure of the domain wall introduced inside junctions is denoted by the magnetic term in Eq. (1), $\boldsymbol{M}\cdot\boldsymbol{\sigma} = M_x\sigma_x + M_y\sigma_y + M_z\sigma_z$, and the magnetization $\boldsymbol{M} = (M_x, M_y, M_z) = M(\sin\theta\sin\varphi_{az}, \sin\theta\cos\varphi_{az}, \cos\theta)$.[62] M is the magnitude of magnetization; θ and φ_{az} are the polar and azimuth angles, describing the orientation of the magnetic moment in the spherical polar coordinate; x is the direction of transport with the origin set in the center of the domain wall, see Fig. 1(a). The magnetization $\boldsymbol{M}$ is homogeneous along the y-direction and points to the $+z$ ($-z$) direction at the $x < 0$ ($x > 0$) side away from the domain wall. Inside the domain wall near $x = 0$, it gradually rotates along the Bloch sphere from the $+z$-direction to the $-z$-direction, holding on the same amplitude M. Thus, the polar angle θ is dependent on the x coordinate as $\cos\theta(x) = -\tanh\frac{x}{L_{\rm dw}}$, where $L_{\rm dw}$ describes the thickness of the domain wall.[62] The azimuth angle φ_{az} of the magnetization is independent of the x coordinate and it describes the configuration of the domain wall. Here, domain walls with $\varphi_{az} = 0$ and $\varphi_{az} = \pi/2$ correspond to the classical Néel-type and Bloch-type configurations, respectively.

To discretize the Hamiltonian in Eq. (1) in a square lattice, we obtain[63]

$$H_{\rm QAHI} = \sum_{\boldsymbol{i}} (\Psi_{\boldsymbol{i}}^\dagger T_0 \Psi_{\boldsymbol{i}} + \Psi_{\boldsymbol{i}}^\dagger T_x \Psi_{\boldsymbol{i}+\delta\boldsymbol{x}} + \Psi_{\boldsymbol{i}}^\dagger T_y \Psi_{\boldsymbol{i}+\delta\boldsymbol{y}} + \text{H.c.}), \quad (2)$$

where $\boldsymbol{i} = (i_x, i_y)$ is the site index. Here $i_y = 1, 2, 3, \ldots, W$ with Wa the width of the QAHI nanoribbon (a the lattice constant) and $i_x = n + 1/2$ with n the integer. The 4×4 matrices $T_{0/x/y}$ are

$$T_0 = \left(m_0 - 4\frac{m_1}{a^2}\right)\tau_x\sigma_0 + \boldsymbol{M}\cdot\boldsymbol{\sigma}, \quad (3)$$

$$T_x = \frac{m_1}{a^2}\tau_x\sigma_0 + \frac{\mathrm{i}v_{\rm F}}{2a}\tau_z\sigma_y, \quad (4)$$

$$T_y = \frac{m_1}{a^2}\tau_x\sigma_0 - \frac{\mathrm{i}v_{\rm F}}{2a}\tau_z\sigma_x. \quad (5)$$

In the following calculation, we set the lattice constant $a = 0.75$, the Fermi velocity $v_{\rm F} = 1$, and the parabolic term $m_1 = 1$.[61]

The targeted QAHI-based Josephson junction is obtained by placing an s-wave superconductor on the QAHI with a continuous domain wall. In the Bogoliubov–de Gennes (BdG) representation, the Hamiltonian of the QAHI-based Josephson junction can be written as follows:[56] $H_{\rm BdG} = \frac{1}{2}\sum_{\boldsymbol{p}} \Phi_{\boldsymbol{p}}^\dagger H_{\rm BdG}(\boldsymbol{p})\Phi_{\boldsymbol{p}}$ with $\Phi_{\boldsymbol{p}} = [(\psi_{\boldsymbol{p},\mathrm{t}\uparrow}, \psi_{\boldsymbol{p},\mathrm{t}\downarrow}, \psi_{\boldsymbol{p},\mathrm{b}\uparrow}, \psi_{\boldsymbol{p},\mathrm{b}\downarrow}), (\psi_{-p,\mathrm{t}\uparrow}^\dagger, \psi_{-p,\mathrm{t}\downarrow}^\dagger, \psi_{-p,\mathrm{b}\uparrow}^\dagger, \psi_{-p,\mathrm{b}\downarrow}^\dagger)]^{\mathrm{T}}$ and

$$H_{\rm BdG}(\boldsymbol{p}) = \begin{pmatrix} H_{\rm QAHI}(\boldsymbol{p}) & \Delta \\ \Delta^\dagger & -H_{\rm QAHI}^*(-p) \end{pmatrix}, \quad (6)$$

where

$$\Delta = \begin{pmatrix} \mathrm{i}\,\mathrm{e}^{\mathrm{i}\varphi_{\mathrm{L(R)}}}\Delta^{\mathrm{t}}\sigma_y & 0 \\ 0 & \mathrm{i}\,\mathrm{e}^{\mathrm{i}\varphi_{\mathrm{L(R)}}}\Delta^{\mathrm{b}}\sigma_y \end{pmatrix}. \quad (7)$$

Here Δ^{t} and Δ^{b} denote the superconducting pairing potential of the top and bottom layers, which are different due to the damping of proximity effect. Set $\Delta^{\mathrm{t}} = \Delta$ and $\Delta^{\mathrm{b}} = 0$. The chemical potential of superconductors is set to be zero. To clarify the topological number of the superconductors with uniform magnetization, we plot the superconducting phase diagram with the boundaries: $\mp\Delta M + M^2 = m_0^2$,[56] see Fig. 1(b). Increasing the induced gap drives the hybrid system going through the phase transition from $\mathcal{N} = 0$ or $\mathcal{N} = 2$ to $\mathcal{N} = 1$, where Chern number $\mathcal{N}$ denotes the number of edge states in the Majorana basis.[64] The $\mathcal{N} = 0$ phase is the trivial superconducting phase without the Majorana edge

modes. However, the $\mathcal{N}=1$ phase is the topological superconductor and carries one chiral Majorana edge mode along the sample edge, and the $\mathcal{N}=2$ phase has two chiral Majorana edge modes and is topologically equivalent to the QAHI phase. Moreover, with a certain induced gap, increasing the magnetization from zero can also lead to the phase transition from $\mathcal{N}=0$ to $\mathcal{N}=1$ and eventually to $\mathcal{N}=2$, as shown in Fig. 1(b).

In the following, we set $\Delta^{\rm t}=\Delta=0.2$ and $\Delta^{\rm b}=0$ and the superconducting pairing potential in the left and right parts picks the same amplitude. Here $\varphi_{\rm L}$ and $\varphi_{\rm R}$ are the superconducting phases in the left and right sides of the junction with $x<0$ and $x>0$, and the superconducting phase difference $\varphi=\varphi_{\rm L}-\varphi_{\rm R}$. Then to discretize the BdG Hamiltonian in a square lattice, $H_{\rm BdG}$ changes to

$$H_{\rm BdG}=H_{\rm QAHI}+\sum_i \Psi_i^\dagger \Delta \Psi_i^\dagger+\sum_i \Psi_i \Delta^\dagger \Psi_i, \tag{8}$$

with the superconducting phase being $\varphi_{\rm L}$ and $\varphi_{\rm R}$ for $i_x\le -1/2$ and $i_x\ge 1/2$, respectively.

Here we first consider that the s-wave superconductor fully covers the entire QAHI nanoribbon with a domain wall structure, which results in the superconducting gap Δ being equal everywhere, i.e. Δ being independent of the site index i. In Section 6, we will study the case that the central region of the QAHI nanoribbon is not covered by the superconductor. Although the inducing superconducting gap Δ is equal everywhere when the QAHI nanoribbon is fully covered by the superconductor, the QAHI-based Josephson junction is not translational invariant along the x-direction due to the domain wall at $x=0$. Therefore it is suitable to be regarded as a Josephson junction, and the present system is similar to the S–S'–S Josephson junction in Refs. [65–68]. Due to the full coverage of the superconductor, the supercurrent can flow through both the conventional s-wave superconductor on the top and the induced superconductor in the QAHI nanoribbon. However, the current flowing through the top is normal Josephson current and the anomalous Josephson current only derives from the QAHI-based superconducting junction. In addition, the present model can also describe the system that the QAHI junction is covered by two separate superconductors but with the slit being narrow, e.g. in the width of several nanometers. Then the induced superconducting pairing potential exists everywhere in the junction and its amplitude Δ is almost independent of the site index i. In this case, the current can only flow through the QAHI-based Josephson junction.

To calculate the current through the QAHI-based Josephson junction at the zero bias, we divide the junction into the left (L) and right (R) parts at $x=0$ such that the total Hamiltonian is expressed as $H_{\rm BdG}=H_{\rm L}+H_{\rm R}+H_{\rm T}$. Here $H_{\rm L}$ ($H_{\rm R}$) is the Hamiltonian of the left (right) region with the index $i_x\le -1/2$ ($i_x\ge 1/2$), and $H_{\rm T}$ denotes the coupling between the left region and the right region, $H_{\rm T}=\sum_{i_y}\Psi^\dagger_{(-1/2,i_y)}T_x\Psi_{(1/2,i_y)}+{\rm H.c.}$ Given the current conservation law, we derive the current formula at the interface of the left and right regions. With the particle number operator of the left part denoted as $\hat{N}_{\rm L}=\sum_{i_x<0,i_y}\Psi^\dagger_{(i_x,i_y)}\Psi_{(i_x,i_y)}$, the current flowing from left to right is expressed as the time evolution of $\hat{N}_{\rm L}$,[69–71]

$$\begin{aligned} I &= e\left\langle \frac{{\rm d}\hat{N}_{\rm L}(t)}{{\rm d}t}\right\rangle=-\frac{{\rm i}e}{\hbar}\left\langle\left[\hat{N}_{\rm L}(t),H_{\rm BdG}(t)\right]\right\rangle \\ &= -\frac{e}{\hbar}\sum_{i_y}{\rm Tr}\left(T_x{\rm i}\left\langle\Psi^\dagger_{(-1/2,i_y)}(t)\otimes\Psi_{(1/2,i_y)}(t)\right\rangle+{\rm H.c.}\right). \end{aligned} \tag{9}$$

Here the operation $\otimes$ denotes the Kronecker product, and to be specific, $\left(\Psi^\dagger_{(-1/2,i_y)}(t)\otimes\Psi_{(1/2,i_y)}(t)\right)_{pq}=\left((\Psi^\dagger_{(-1/2,i_y)}(t)\right)_q\left(\Psi_{(1/2,i_y)}(t)\right)_p$. The averaged quantity $i\left\langle\Psi^\dagger_{(-1/2,i_y)}(t)\otimes\Psi_{(1/2,i_y)}(t)\right\rangle$ can be expressed in terms of the nonequilibrium Keldysh Green's functions $G^<_{{\rm RL},11}(t,t;i_y,i_y)$. For the superconducting state, it is convenient to introduce the BdG representation in which $\boldsymbol{G}^<_{\rm RL}$ adopts the form[72]

$$\begin{aligned} &\boldsymbol{G}^<_{\rm RL}\left(t,t';i_y,i'_y\right) \\ &={\rm i}\left\langle\begin{pmatrix}\Psi^\dagger_{(-1/2,i'_y)}(t') & \Psi^{\rm T}_{(-1/2,i'_y)}(t')\end{pmatrix}\otimes\begin{pmatrix}\Psi_{(1/2,i_y)}(t)\\ \Psi^{\dagger{\rm T}}_{(1/2,i_y)}(t)\end{pmatrix}\right\rangle. \end{aligned} \tag{10}$$

Then in terms of $\boldsymbol{G}^<_{\rm RL}$, the current is given by

$$\begin{aligned} I=&-\frac{e}{\hbar}\sum_{i_y}{\rm Tr}(T_{\rm LR}\boldsymbol{G}^<_{\rm RL}(t,t;i_y,i_y) \\ &-\boldsymbol{G}^<_{\rm LR}(t,t;i_y,i_y)T_{\rm RL}), \end{aligned} \tag{11}$$

where $T_{\rm LR}=\begin{pmatrix}1&0\\0&0\end{pmatrix}\otimes T_x$ and $T_{\rm RL}=\begin{pmatrix}1&0\\0&0\end{pmatrix}\otimes T_x^\dagger$.

As to the determination of these nonequilibrium Green's functions $\boldsymbol{G}^<$, they can be obtained from the retarded and advanced Green's functions. When Fourier transformed, $\boldsymbol{G}^<_{\rm LR}(\varepsilon)=\boldsymbol{G}^{\rm r}_{\rm LL}(\varepsilon)\hat{T}_x\boldsymbol{g}^<_{\rm RR}(\varepsilon)+\boldsymbol{G}^<_{\rm LL}(\varepsilon)\hat{T}_x\boldsymbol{g}^{\rm a}_{\rm RR}(\varepsilon)$, where $\hat{T}_x=\begin{pmatrix}T_x&0\\0&-T_x^*\end{pmatrix}$. The retarded and advanced Green's functions are defined as $\boldsymbol{g}^{\rm r}_{\rm LL}(\varepsilon)=[\boldsymbol{g}^{\rm a}_{\rm LL}(\varepsilon)]^\dagger=[\varepsilon\boldsymbol{I}-H_{\rm L}+{\rm i}\eta]^{-1}$. Here η is a small energy relaxation rate which takes into account the damping of quasiparticle states due to the inelastic process inside the electrodes.[73] $\boldsymbol{G}^{\rm r}_{\rm LL}(\varepsilon)=\left[[\mathrm{g}^{\rm r}_{\rm LL}]^{-1}-\hat{T}_x\boldsymbol{g}^{\rm r}_{\rm RR}\hat{T}_x^\dagger\right]^{-1}$ and $\boldsymbol{G}^{\rm a}_{\rm LL}(\varepsilon)=[\boldsymbol{G}^{\rm r}_{\rm LL}(\varepsilon)]^\dagger$. Since there is no bias voltage, $\boldsymbol{g}^<_{\rm RR}(\varepsilon)=-f(\varepsilon)[\boldsymbol{g}^{\rm r}_{\rm RR}(\varepsilon)-\boldsymbol{g}^{\rm a}_{\rm RR}(\varepsilon)]$ and $\boldsymbol{G}^<_{\rm LL}(\varepsilon)=-f(\varepsilon)[\boldsymbol{G}^{\rm r}_{\rm LL}(\varepsilon)-\boldsymbol{G}^{\rm a}_{\rm LL}(\varepsilon)]$ according to the fluctuation-dissipation theorem, where $f(\varepsilon)$ is the Fermi distribution function at energy ε and at zero temperature. Also, $\boldsymbol{G}^<_{\rm RL}(\varepsilon)$ can be derived in the similar procedure, just by interchanging the subscripts L and R. Eventually, the supercurrent in QAHI-based junction, denoted as I, is

$$I=-\frac{e}{h}\int{\rm d}\varepsilon{\rm Tr}\left[T_{\rm LR}\boldsymbol{G}^<_{\rm RL}(\varepsilon)-\boldsymbol{G}^<_{\rm LR}(\varepsilon)T_{\rm RL}\right]. \tag{12}$$

3. Occurrence of anomalous current

We find that the anomalous current appears in the QAHI-based Josephson junction in Fig. 1. The current-phase relations calculated in Fig. 2 directly show that the non-zero supercurrent may occur with zero superconducting phase difference. Two key factors of domain walls play roles: the magnetization amplitude M and the configuration depending on the azimuth angle φ_{az}. The nonzero magnetization of domain walls is a necessary condition and positively impacts the value of the anomalous current by comparing Figs. 2(a)–2(d). The standard sinusoidal curve with $M = 0$ in Fig. 2(a) refers to the normal Josephson junction without domain walls. Since the magnetization $M = 0.05$, $M = 0.2$, and $M = 0.35$ in Figs. 2(b), 2(c), and 2(d) correspond to the $\mathcal{N} = 0$, $\mathcal{N} = 1$, and $\mathcal{N} = 2$ superconducting phases [see Fig. 1(b)], the anomalous Josephson current appears for all the three superconducting phases, indicating that the anomalous Josephson current is independent of the superconducting phase. The QAHI-based Josephson junction with Bloch-type domain wall ($\varphi_{az} = \pi/2$) presents the most significant anomalous Josephson effect whereas the Néel-type one ($\varphi_{az} = 0$) shows no anomalous current. With the increase of the azimuth angle φ_{az} from 0 to $\pi/2$, the anomalous supercurrent (i.e. the current I at the phase difference $\varphi = 0$) increases and the current-phase relation holds a sinusoidal function in the period of 2π [see Figs. 2(b)–2(d)]. Thus, the properties of the domain wall (M and φ_{az}) are of vital importance to produce the anomalous current.

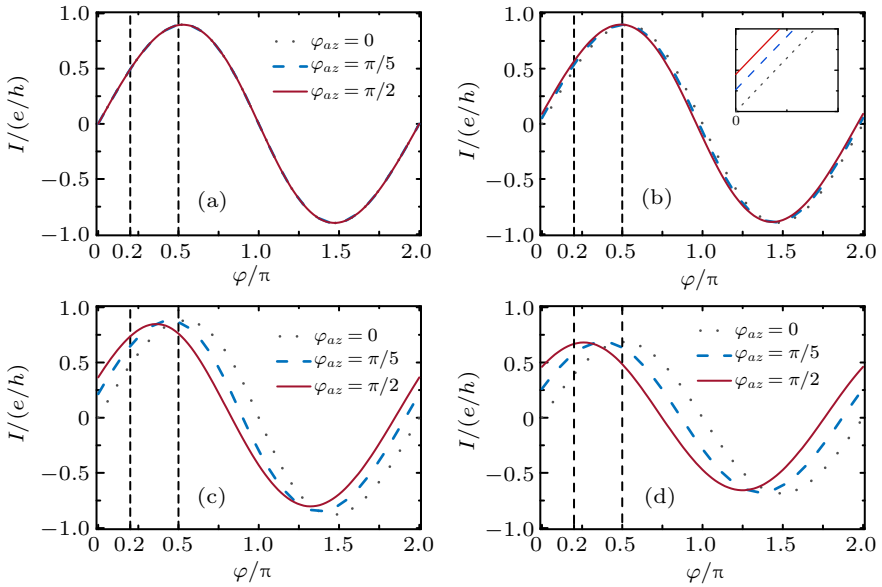

Fig. 2. Current–phase relations, i.e., the current I versus the superconducting phase difference φ with the magnetization $M = 0$ (a), 0.05 (b), 0.2 (c), and 0.35 (d). Different curves correspond to different azimuth angles $\varphi_{az} = 0$, $\pi/5$, and $\pi/2$. The vertical dashed lines mark $\varphi = \pi/5$ and $\pi/2$. The inset in (b) amplifies the current around $\varphi = 0$ to highlight the anomalous current. Other parameters are the nanoribbon width $W = 80$ and thickness of the domain wall $L_{\rm dw} = 3$.

Let us study the dependence of the anomalous current on the azimuth angle φ_{az} at the zero phase difference. Figure 3(a) shows the anomalous current exists if $\varphi_{az} \neq 0$ and $\varphi_{az} \neq \pi$. When $\varphi_{az} \in (0, \pi)$, the anomalous current I is positive, indicating a positive phase shift of the current-phase relation. However, when $\varphi_{az} \in (\pi, 2\pi)$, both the anomalous current I and the phase shift are negative. In addition, the larger the magnetization M is, the greater the anomalous current I is. Here the supercurrent $I(\varphi = 0, \varphi_{az})$ oscillates sinusoidally in 2π period and it is an odd function of φ_{az}, satisfying

$$I(\varphi = 0, \varphi_{az}) = -I(\varphi = 0, -\varphi_{az}). \tag{13}$$

The azimuth angle φ_{az} also influences the supercurrent I of QAHI-based Josephson junctions at nonzero phase difference $\varphi = \pi/5$, $\pi/2$, π, and $3\pi/2$ shown in Figs. 3(b)–3(e). When the magnetization $M = 0$, the current is independent of φ_{az}. When $M \neq 0$, the azimuth angle arouses the oscillation of the supercurrent $I(\varphi, \varphi_{az})$ at a certain phase difference. With the increase of M, the oscillating amplitude of the current versus φ_{az} increases. When φ near 0, the oscillating period of the current versus φ_{az} is 2π as shown in Fig. 3(b). However, when $\varphi = \pi/2$ or near $\pi/2$, the oscillating period seems to be π [see Fig. 3(c)]. Here the curves in Fig. 3 are in accord with those in Fig. 2, e.g., see the curves in Fig. 3(b) [Fig. 3(c)] at $M = 0.2$ (colored purple) and the currents along the vertical dashed lines at $\varphi = \pi/5$ [$\pi/2$] in Fig. 2(c). In addition, the behaviors of the current for the $\mathcal{N} = 0$, $\mathcal{N} = 1$, and $\mathcal{N} = 2$ superconducting phases are not essentially different. Furthermore, from numerical results [e.g. by comparing Fig. 3(a) with 3(d) and Fig. 3(c) with 3(e)], the supercurrent has the exact relations

$$I(\varphi, \varphi_{az}) = -I(-\varphi, -\varphi_{az}), \tag{14}$$

$$I(\varphi,\varphi_{az}) = I(\varphi+2\pi,\varphi_{az}), \tag{15}$$

$$I(\varphi,\varphi_{az}) = I(\varphi,\varphi_{az}+2\pi). \tag{16}$$

We briefly conclude that the anomalous current of QAHI-based Josephson junctions will occur if the domain wall structure satisfies $M \neq 0$ and $\varphi_{az} \neq 0$ and π. The requirement of nonzero M is reasonable, otherwise the device reverts to a normal Josephson junction. It should be noticed that why the Néel-type domain wall does not contribute to the anomalous current and where the relation in Eq. (14) roots remain further discussions.

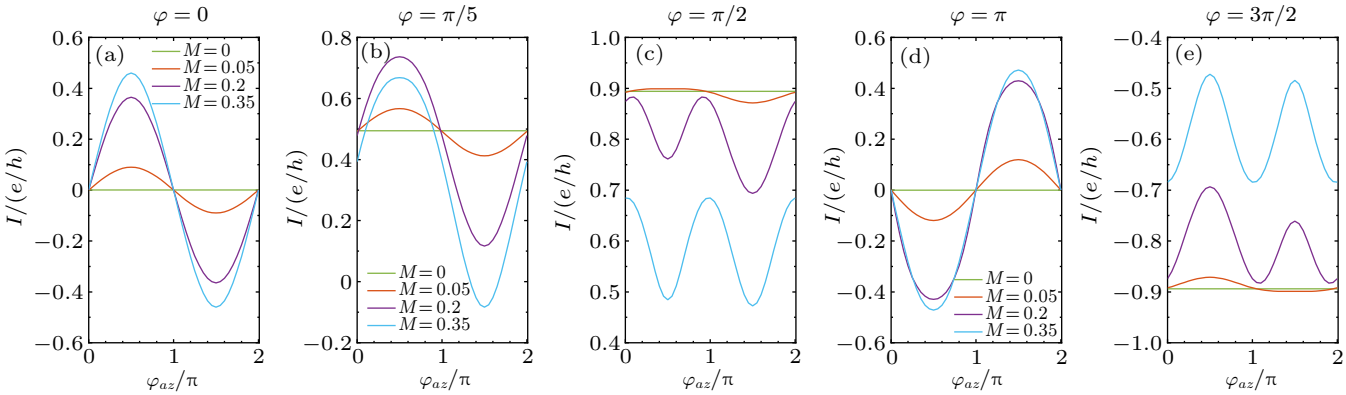

Fig. 3. Supercurrent I versus the azimuth angle φ_{az}, corresponding to $\varphi = 0$ (a), $\pi/5$ (b), $\pi/2$ (c), π (d), and $3\pi/2$ (e). Curves in different colors represent different values of magnetization $M = 0$, 0.05, 0.2, and 0.35. All parameters unmentioned are the same as those in Fig. 2.

4. Analysis of symmetry

In this section, we figure out the broken symmetry needed for the anomalous current by applying symmetry analysis to the Hamiltonian of the QAHI-based Josephson junction. Besides the non-equilibrium Green's method in Eq. (12), the supercurrent through the QAHI-based Josephson junction could also be theoretically obtained via the thermodynamic relation

$$I(\varphi) = \frac{2e}{\hbar}\frac{\partial F}{\partial \varphi}, \tag{17}$$

where F denotes the free energy of the junction, $F = -T\ln\mathrm{Tr}[\mathrm{e}^{-H_{\mathrm{BdG}}(\varphi)/T}]$ with the temperature T.

In order to obtain the anomalous current, $I(\varphi = 0) \neq 0$, the free energy is requested to be not symmetric under the transformation of superconducting phase $\varphi \to -\varphi$. If $F(-\varphi) = F(\varphi)$, then $I(-\varphi) = -I(\varphi)$ will come and no anomalous current will exit. Therefore, once finding out a unitary transformation U such that

$$UH_{\mathrm{BdG}}(\varphi)U^{\dagger} = H_{\mathrm{BdG}}(-\varphi), \tag{18}$$

the anomalous current is zero, then we can determine the necessary condition for the appearance of the anomalous current.

In two-dimensional systems, there are three kinds of symmetry operations:[74] (i) spatial inversion operations R_x, R_y, and R_z act on the coordinates of Hamiltonians, that is, R_x transforms x to $-x$; (ii) spin rotation operations σ_x, σ_y, and σ_z act in the spin space, e.g., σ_x transforms $\sigma_x \to \sigma_x$, $\sigma_y \to -\sigma_y$, $\sigma_z \to -\sigma_z$; (iii) the time-reversal operation, denoted as $\mathcal{T} = \mathrm{i}\sigma_y\mathcal{K}$, where $\mathcal{K}$ is the complex conjugate operator. These symmetry operations and their composition serve as the candidates for U.

We first analyze how the U transforms the QAHI-based Josephson junction with an abrupt domain wall. The Hamiltonian H_{BdG} can be rewritten as $H_{\mathrm{BdG}}(\varphi) = H_{\mathrm{QAHI}} + H_{\Delta}(\varphi)$, where the magnetic term of H_{QAHI} is described by $\boldsymbol{M}\cdot\boldsymbol{\sigma} = M[\Theta(-x) - \Theta(x)]\tau_0\sigma_z$, with Θ being the Heaviside function. Rewrite the superconducting pairing potential in Eq. (6) in the direct product space of the particle-hole, layer, and spin spaces,

$$\begin{aligned} H_{\Delta}(\varphi) &= \begin{pmatrix} 0 & \Delta \\ \Delta^{\dagger} & 0 \end{pmatrix} \\ &= \Theta(-x)\left(-\cos\frac{\varphi}{2}\zeta_y + \sin\frac{\varphi}{2}\zeta_x\right) \\ &\quad \otimes\frac{1}{2}[(\Delta_{\mathrm{t}}+\Delta_{\mathrm{b}})\tau_0 + (\Delta_{\mathrm{t}}-\Delta_{\mathrm{b}})\tau_z)] \otimes \sigma_y \\ &\quad + \Theta(x)\left(-\cos\frac{\varphi}{2}\zeta_y - \sin\frac{\varphi}{2}\zeta_x\right) \\ &\quad \otimes\frac{1}{2}[(\Delta_{\mathrm{t}}+\Delta_{\mathrm{b}})\tau_0 + (\Delta_{\mathrm{t}}-\Delta_{\mathrm{b}})\tau_z)] \otimes \sigma_y, \end{aligned} \tag{19}$$

where $\zeta_{x,y,z}$ is the Pauli matrix acting on the particle-hole space, and the superconducting phases of the left and right parts are chosen as $\varphi_{\mathrm{L}} = -\frac{\varphi}{2}$ and $\varphi_{\mathrm{R}} = \frac{\varphi}{2}$ without loss of generality. After testing the symmetry operations in all possible arrangements like R_x, $\sigma_y R_y$, $\sigma_x R_z \mathcal{T}$, etc., the unitary transformation $U = \sigma_y R_y \mathcal{T}$ satisfies Eq. (18). Thus, there is no anomalous current in the QAHI-based junction with an abrupt domain wall.

Next we discuss the QAHI-based Josephson junction with a continuous domain wall structure. The Hamiltonian is explicitly composed of $p_y\sigma_x$, $p_y\sigma_x$, $m(\boldsymbol{p})\sigma_0$, the magnetic term $\boldsymbol{M}\cdot\boldsymbol{\sigma} = M_x(x)\sigma_x + M_y(x)\sigma_y + M_z(x)\sigma_z$, and the pairing term $\mathrm{H}_{\Delta}(\varphi)$. Table 1 summarizes how each part of the Hamiltonian transforms when we apply the unitary transformation

$U=\sigma_y R_y \mathcal{T}$. Here the terms ($p_x\sigma_y$ and $m(\boldsymbol{p})\sigma_0$), which are not listed in Table 1, remain unchanged under the unitary transformation σ_y, R_y and $\mathcal{T}$. Although magnetic terms $M_x\sigma_x$ and $M_z\sigma_z$ break the isolated symmetry σ_y or R_y, they preserve the combined symmetry $\sigma_y R_y \mathcal{T}$. It is the y-component of magnetization that breaks $\sigma_y R_y \mathcal{T}$: $M_y \to -M_y$ under $U=\sigma_y R_y \mathcal{T}$, that is,

$$\sigma_y R_y \mathcal{T} H_{\mathrm{BdG}}(\varphi,\varphi_{az})[\sigma_y R_y \mathcal{T}]^{\dagger} = H_{\mathrm{BdG}}(-\varphi,-\varphi_{az}). \quad (20)$$

Therefore, the anomalous current has the property $I(\varphi,\varphi_{az}) = -I(-\varphi,-\varphi_{az})$ as shown in Eq. (14).

Table 1. Symmetry operations on Hamiltonian. Here we take "–" to represent that the Hamiltonian term remains unchanged under the corresponding symmetry operation.

	$U=\sigma_y R_y \mathcal{T}$		
	$\mathcal{T}$	R_y	σ_y
$H_\Delta(\varphi)$	$H_\Delta(-\varphi)$	–	–
$p_y\sigma_x$	–	$-p_y\sigma_x$	$-p_y\sigma_x$
$M_z(x)\sigma_z$	$-M_z(x)\sigma_z$	–	$-M_z(x)\sigma_z$
$M_x(x)\sigma_x$	$-M_x(x)\sigma_x$	–	$-M_x(x)\sigma_x$
$M_y(x)\sigma_y$	$-M_y(x)\sigma_x$	–	–

Recalling that $\varphi_{az}=0$ and π correspond to $M_x\neq 0$ and $M_y=0$, it is unsurprising that there will be no anomalous current protected by symmetry $U=\sigma_y R_y \mathcal{T}$ in the Néel-type domain wall even if the magnetization amplitude is nonzero. Thus, the M_y component of a domain wall is indispensable to the occurrence of the anomalous current.

5. Manipulation of the phase shift

As before, we display the existence and the origin of the anomalous Josephson current together with the observable phase shift. In this section, we quantify how the anomalous Josephson effect is affected by systematic parameters: the azimuth angle φ_{az}, the amplitude of magnetization M, the thickness of a domain wall L_{dw}, and the width of the QAHI-based junction W.

From now on, we precisely calculate the phase shift δ of the supercurrent from current-phase relations as shown in Fig. 2 via Fourier transformation. After taking the Fourier transformation, the supercurrent can be expressed as

$$I(\varphi)=\sum_{n=1}^{\infty} A_n \sin(n\varphi+\delta_n),$$

where the amplitude and the phase shift can be obtained from $A_n=\sqrt{a_n^2+b_n^2}$ and $\delta_n=\arctan(b_n/a_n)$, with

$$a_n=\frac{1}{\pi}\int_0^{2\pi} I(\varphi)(\sin n)\varphi\,\mathrm{d}\varphi, \quad (21)$$

$$b_n=\frac{1}{\pi}\int_0^{2\pi} I(\varphi)(\cos n)\varphi\,\mathrm{d}\varphi. \quad (22)$$

Hereafter we focus on the first-order frequency component, the amplitude A_1 and the phase shift $\delta=\delta_1$. The high-order frequency components are ignored since the 2nd-order frequency component contributes less than one percent to the supercurrent.

We first find that the azimuth angle φ_{az} of a domain wall periodically modulates the phase shift δ and the amplitude A_1 of the supercurrent. The phase shift oscillates versus the azimuth angle in the period of 2π and is an odd function, i.e. $\delta(-\varphi_{az})=-\delta(\varphi_{az})$, as shown in Figs. 4(a) and 4(c). The sinusoidal oscillation of δ versus φ_{az} is rooted in the varying magnetic components, $M_y=M\sin\theta\sin\varphi_{az}$ and $M_x=M\sin\theta\cos\varphi_{az}$. Roughly to say, the phase shift δ is proportional to M_y component of the magnetization. Since $M_y\sim\sin\varphi_{az}$, the phase shift $\delta\sim\sin\varphi_{az}$. Similarly, the amplitude A_1 also oscillates versus the azimuth angle. However, the period is π rather than 2π and A_1 is an even function of φ_{az}, as shown in Figs. 4(b) and 4(d). Based on the antisymmetry of supercurrent in Eq. (14) combined with Eqs. (21) and (22), we can straightforwardly obtain the odd-even relation $A_1(-\varphi_{az})=A_1(\varphi_{az})$ and $\delta(-\varphi_{az})=-\delta(\varphi_{az})$.

Figure 4 also shows that varying the magnetization M and the junction width W can preserve the periodic and odd-even properties of $\delta(\varphi_{az})$ and $A_1(\varphi_{az})$ but influence the oscillating amplitude. With non-zero magnetization, the phase shift always peaks at $\varphi_{az}=\pi/2$, confirming that the Bloch-type domain wall is preferable for the anomalous Josephson effect. Thus, we define the maximum values of phase shift and supercurrent amplitude as $\delta_{\max}=\delta(\varphi_{az}=\pi/2)$ and the corresponding supercurrent amplitude is $A_{\mathrm{m}}=A_1(\varphi_{az}=\pi/2)$. In the following, we study to which extent $\delta_{\max}$ and A_{m} could be tuned by other parameters of the QAHI-based junction with a Bloch-type domain wall.

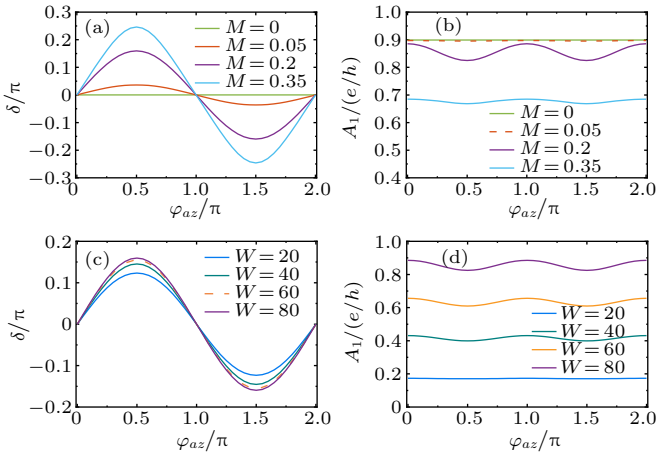

Fig. 4. Phase shift δ and amplitude A_1 versus the azimuth angle φ_{az} in QAHI-based Josephson junction, calculated from Eqs. (21) and (22). [(a), (b)] Curves with different magnetization $M=0$, 0.05, 0.2, 0.35 and other parameters $L_{\mathrm{dw}}=3$ and $W=80$. [(c), (d)] Curves with different widths $W=20$, 40, 60, 80 and other parameters $L_{\mathrm{dw}}=3$ and $M=0.2$.

Overall, the increasing magnetization M strengthens the maximum phase shift $\delta_{\max}$ but weakens the supercurrent am-

plitude $A_{\rm m}$, as shown in Figs. 5 and 6. The maximum phase shift $\delta_{\rm max}$ is nearly proportional to the magnetization M. When M increases, the component M_y increases and effectively devotes to the anomalous Josephson current. Also, curves of $\delta_{\rm max}(M)$ are continuous and smooth without abrupt change points [see Figs. 5(a) and 6(a)] even if the superconducting state varies from the $\mathcal{N}=0$ phase through $\mathcal{N}=1$ phase to $\mathcal{N}=2$ phase, i.e., the bulk gap closes and opens twice, when M increases from 0 to 0.5. Actually, in the superconducting junction, what mainly carries the current is neither edge states nor bulk states. In the two superconducting leads with $x \ll 0$ or $x \gg 0$, the dominant carrier is Cooper pairs leading to the non-dissipative supercurrent. The edge states can also give rise to current but not so much. The bulk states above the gap correspond to the quasiparticles being scattered, not leading to supercurrent. Around the central region with a domain wall, the current comes from the Andreev bound states.[75] Due to the supercurrent carried by the Cooper pairs in the superconducting leads and by the Andreev bound states in the junction region, this leads to a large Josephson current in the $\mathcal{N}=0$ phase and the smooth curves of $\delta_{\rm max}(M)$ for the superconducting state varying from the $\mathcal{N}=0$ phase through $\mathcal{N}=1$ phase to the $\mathcal{N}=2$ phase. In addition, with the increase of the magnetization, the supercurrent amplitude $A_{\rm m}$ slightly decreases but still keeps a large value as shown in Figs. 5(b) and 6(b).

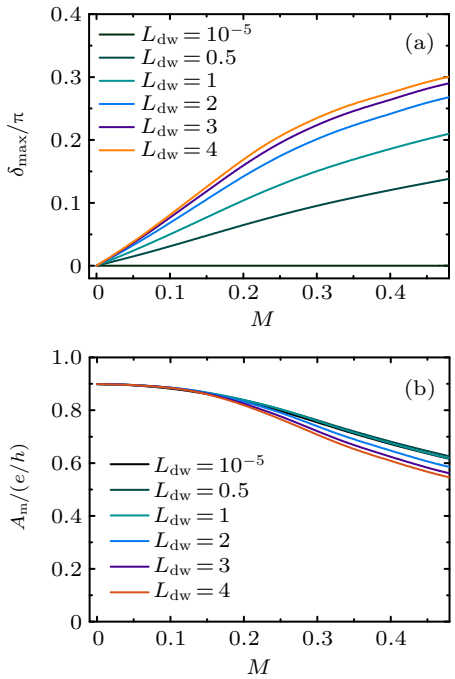

Fig. 5. The maximum phase shift $\delta_{\rm max}$ (a) and supercurrent amplitude $A_{\rm m}$ (b) versus magnetization M in the Bloch-type domain wall ($\varphi_{az}=\pi/2$). Different curves label different thicknesses of a domain wall $L_{\rm dw}=10^{-5}$, 0.5, 1, 2, 3, and 4. All parameters unmentioned are the same as those in Fig. 2.

Figures 5(a) and 5(b) show the maximum phase shift $\delta_{\rm max}$ and the supercurrent amplitude $A_{\rm m}$ for the different thickness $L_{\rm dw}$ of the domain wall. The maximum phase shift is strongly affected by the thickness $L_{\rm dw}$. Explicitly, $L_{\rm dw}\to 0$ describes an abrupt domain wall where $\boldsymbol{M}=(0,0,M[\Theta(-x)-\Theta(x)])$. In such a case, even if $M\neq 0$, no anomalous current can exist and $\delta_{\rm max}=0$, as depicted by the horizontal straight line in Fig. 5(a), that is, at $L_{\rm dw}\to 0$, $I(\varphi=0,\varphi_{az})=0$ for any azimuth angle φ_{az}. When $L_{\rm dw}\neq 0$, the magnetization in the domain wall gradually changes from $+z$-direction to $-z$-direction, implying the nonzero M_y in the Bloch-type configuration. Thus, the maximum phase shift $\delta_{\rm max}$ appears. The larger the thickness $L_{\rm dw}$ is, the greater the $\delta_{\rm max}$ grows [see Fig. 5(a)], because the $\int M_y(x)\,{\rm d}x$ has a larger value corresponding to a larger $L_{\rm dw}$. Here both the magnetization M and the thickness $L_{\rm dw}$ are positively correlated with the quantity $\int M_y(x)\,{\rm d}x$, which is the key factor to cause the anomalous current in QAHI-based Josephson junctions. On the other hand, the thickness $L_{\rm dw}$ shows tiny effects on the supercurrent amplitude [see Fig. 5(b)]. With the increase of the thickness $L_{\rm dw}$, the amplitude $A_{\rm m}$ slightly decreases only.

The width of a QAHI-based Josephson junction has minor influence in the maximum phase shift $\delta_{\rm max}$ but significant influence in the supercurrent amplitude $A_{\rm m}$. The maximum phase shift $\delta_{\rm max}$ is not sensitive to the width W [see Fig. 6(a)]. Except for the very small width $W=20$, the curves of $\delta_{\rm max}$ versus the magnetization M for the width $W=40$, 60 and 80 are almost overlapped together. On the other hand, the increasing width W boosts the supercurrent amplitude $A_{\rm m}$ as shown in Fig. 6(b). Here $A_{\rm m}$ is approximately proportional to the width W. The wider the nanoribbon is, the more supercurrent it can carry, which benefits the experimental detection of the anomalous Josephson effect.

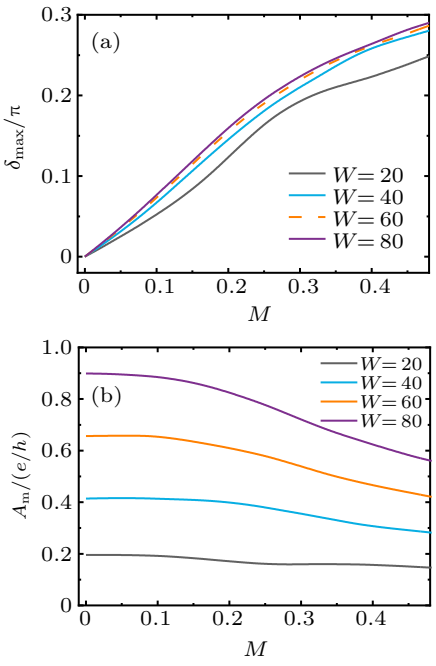

Fig. 6. The maximum phase shift $\delta_{\rm max}$ (a) and amplitude of supercurrent $A_{\rm m}$ (b) versus magnetization M in the Bloch-type domain wall ($\varphi_{az}=\pi/2$). Different curves label different widths of junction $W=20$, 40, 60, and 80. All parameters unmentioned are the same as those in Fig. 2.

To demonstrate the important effect of the component M_y of magnetization rather than the component M_z on the amount of the anomalous current, we propose other paths depicting how the magnetization from $+z$-direction on the left side transits into $-z$-direction on the right side. Here the azimuth angle is set to be $\varphi_{az} = \pi/2$ to study the maximum phase shift $\delta_{\max}$ in the Bloch-type domain wall. The magnetization is set $\boldsymbol{M} = (0, \alpha M \sin\theta, M\cos\theta)$ with $M_y = \alpha M \sin\theta$ and $\cos\theta(x) = -\tanh\frac{x}{L_{\rm dw}}$. The projection of magnetization in the y–z plane is a semi-ellipse as shown in the inset of Fig. 7(b). The coefficient α changes the M_y but keeps M_z. When $\alpha = 1$, the absolute value of magnetization $\boldsymbol{M}$ is constant inside the domain wall as discussed above. Figure 7(a) shows that the maximum phase shift $\delta_{\max}$ strongly depends on the coefficient α: (i) for $\alpha = 0$, $\delta_{\max}$ is zero regardless of the magnetization M, because of $M_y = 0$; (ii) for $\alpha < 1$, $\delta_{\max}$ is less than the former case with $\alpha = 1$; (iii) for $\alpha > 1$, $\delta_{\max}$ is larger than that of $\alpha = 1$. Approximately, the maximum phase shift $\delta_{\max}$ is proportional to the α, i.e., M_y. It is confirmed that the component M_y of the magnetization is the key factor to lead to the anomalous current again. On the other hand, the amplitude of supercurrent $A_{\rm m}$ weakly relies on α [see Fig. 7(b)]. With the growth of α (M_y), the supercurrent amplitude slightly reduces, but $A_{\rm m}$ still has a large value.

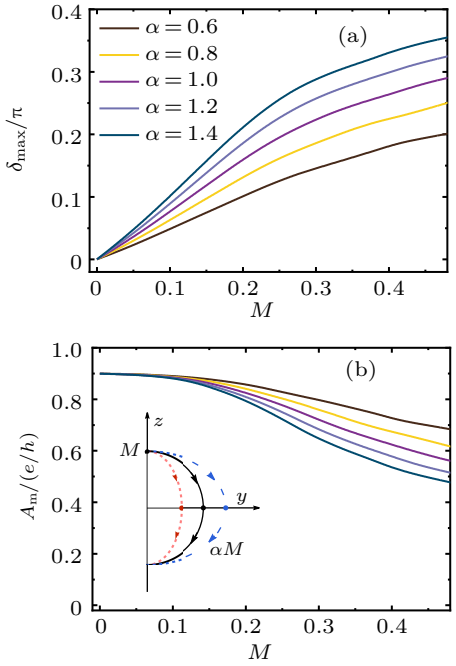

Fig. 7. The maximum phase shift $\delta_{\max}$ (a) and amplitude of supercurrent $A_{\rm m}$ (b) versus magnetization M in the Bloch-type domain wall ($\varphi_{az} = \pi/2$). Different curves label different paths with coefficients $\alpha = 0.6$, 0.8, 1, 1.2, and 1.4. The inset in (b) shows the projection of magnetization in the y–z plane. All parameters unmentioned are the same as those in Fig. 2.

Thus, we briefly claim that the azimuth angle, which determines the configuration of the domain wall, periodically regulates the anomalous current in both the phase shift and the current amplitude. In the Bloch-type domain wall, the maximum phase shift could be enlarged by increasing the magnetization or thickening the domain wall; the supercurrent amplitude could be boosted by widening the junction.

6. QAHI-based anomalous Josephson junction with bare QAHI layers and 0–π junction transition

So far, we have discussed the Josephson junction where the superconductor covers the entire QAHI nanoribbon with a domain wall structure. In this case, the supercurrent can directly flow through the superconductor and it is very large. In order to further enhance the phase shift, in this section we consider a QAHI-based Josephson junction with bare layers, i.e., the central region of the QAHI nanoribbon is not covered by superconductor, as shown in Fig. 8(a). That is to say, we consider a long Josephson junction.[11,65,76] The Hamiltonian is the same as Eq. (8) except that the superconducting pairing potentials Δ are 0 when $(-L_{\rm Q} + 1/2) \le i_x \le (L_{\rm Q} - 1/2)$. Here $2L_{\rm Q}$ denotes the number of bare QAHI layers. We calculate the supercurrent by Eq. (12), the maximum phase shift $\delta_{\max}$ by Eq. (21), and the amplitude $A_{\rm m}$ by Eq. (22).

In addition, the supercurrent can also be obtained from the energy spectrum as a function of the superconducting phase difference φ, in which the Andreev bound states appear in the bulk gap of the left and right superconducting leads. The supercurrent flowing through the Josephson junction is mainly carried by the Andreev bound states. For the Néel-type domain wall with the azimuth angle $\varphi_{az} = 0$, the energy spectrum exhibits symmetry versus the phase difference φ, which results in the supercurrent being 0 at $\varphi = 0$. That is, the anomalous Josephson current disappears for the Néel-type domain wall. On the other hand, while the azimuth angle $\varphi_{az} \neq 0$ (e.g. the Bloch-type domain wall with $\varphi_{az} = \pi/2$), the aforementioned symmetry is broken via the non-zero component M_y of magnetization, and the energy spectrum at $-\varphi$ is not equal to that at φ as usual. This leads to the anomalous Josephson current.

Similar to the superconducting full coverage case, the phase shift δ of the anomalous current shows a sinusoidal relation to the azimuth angle φ_{az}, and δ reaches the maximum value in the Bloch-type domain wall with $\varphi_{az} = \pi/2$. Figures 8(b) and 8(c) show the maximum phase shift and the supercurrent amplitude at $\varphi_{az} = \pi/2$ with the existence of bare QAHI layers. For comparison, we also plot the curve with no bare QAHI layers, marked by $L_{\rm Q} = 0$, which has been studied in the above section.

The supercurrent amplitude $A_{\rm m}$ is insensitive to the change of magnetization M. As M increases, $A_{\rm m}$ slightly reduces: $A_{\rm m}$ at $M = 0.45$ is about 70% of that at $M = 0$. With the increase of the number of bare layers, the supercurrent amplitude $A_{\rm m}$ strongly reduces, which is similar to the previous results in the long Josephson junction.[11,65,76]

Nonetheless, even for $L_Q = 4$ (i.e. with 8 bare QAHI layers), the supercurrent amplitude A_m still maintains the value about $0.04A_m(L_Q = 0)$, which is measurable in experiments. In addition, the increase of junction width can significantly enlarge the amplitude of supercurrent but keep the amount of the phase shift.

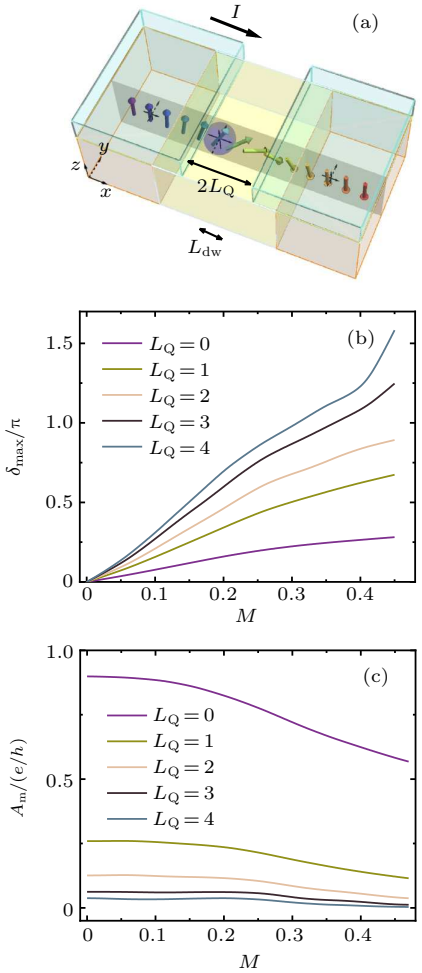

Fig. 8. (a) Schematic diagram for the QAHI-based Josephson junction with bare QAHI layers. The domain wall structure is gradually rotating along the x direction, plotted by vectors pointing the orientation of magnetization. Note: the illustration is not drawn to scale; in practice, the thickness of a domain wall L_{dw} is much smaller than the size of junction. The maximum phase shift δ_{max} (b) and amplitude of supercurrent A_m (c) versus magnetization M in the Bloch-type domain wall ($\varphi_{az} = \pi/2$). Different curves label the different numbers of the bare QAHI layer L_Q. All parameters unmentioned are the same as those in Fig. 2.

The maximum phase shift δ_{max} monotonically increases still as the magnetization M increases, and δ_{max} is positively correlated with M, see Fig. 8(b). Notably, the existence of bare QAHI layers ($L_Q \neq 0$) dramatically enhances the maximum phase shift δ_{max}. Since the direct tunneling of Cooper pairs from the left side to the right side strongly reduces, the component of anomalous current obviously rises. The more the L_Q increases, the larger the δ_{max} becomes. With the magnetization $M = 0.45$, the maximum phase shift exceeds π for $L_Q = 3$ and 4. This allows us to achieve a continuous regulation between the 0 junction and the π junction via tuning the magnetization or the azimuth angle.

In order to clearly show the continuous transition between 0 and π Josephson junctions, Fig. 9 shows the current-phase relation, I–φ, for the different magnetization M at $\varphi_{az} = \pi/2$. When $M = 0$, the supercurrent equals $I = I_c \sin\varphi$ and presents a normal Josephson junction (or 0 junction) with $\delta = 0$. When M increases, the phase shift δ rises from 0, the curve of I–φ gradually shifts to the left, and the current-phase relation is $I = I_c \sin(\varphi + \delta)$, denoted as the anomalous junction, see curves with $M = 0.17$ and 0.27 in Fig. 9(a) and $M = 0.07$ and 0.2 in Fig. 9(b). When M further increases to a certain value, the supercurrent equals $I = I_c \sin(\varphi + \pi)$ and presents a π Josephson junction with $\delta = \pi$, see the curves with $M = 0.37$ in Fig. 9(a) and $M = 0.32$ in Fig. 9(b). Therefore, by tuning the magnetization M, we can continuously change between the 0 and π junction. Moreover, since the maximum phase shift at $\varphi_{az} = \pi/2$ could reach or exceed π, it is also possible to continuously achieve the 0–π transition of Josephson junction via regulating the azimuth angle φ_{az} of the domain wall.

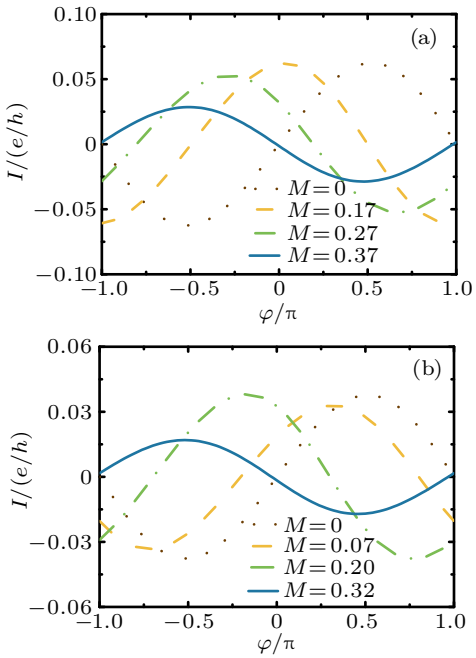

Fig. 9. Continuous transition from 0 junction to π junction in QAHI-based Josephson junction with bare QAHI layers. The supercurrent I versus the phase difference φ with (a) $L_Q = 3$ and (b) $L_Q = 4$ in the Bloch-type domain wall ($\varphi_{az} = \pi/2$). Different curves correspond to different magnetization $M = 0, 0.17, 0.27, 0.37$ in (a) and $M = 0, 0.07, 0.2, 0.32$ in (b). All parameters unmentioned are the same as those in Fig. 2.

7. Discussion and conclusion

In summary, we have studied the Josephson effect in the system consisting of the quantum anomalous Hall insulator nanoribbon with a domain wall structure covered by the superconductor. The current–phase relation shows the occurrence of the anomalous Josephson current under the condition that the magnetization is nonzero and the azimuth angle of the domain wall is neither 0 nor π. Through the symmetry analysis of Hamiltonians, the y-direction component M_y of the magnetization is the key factor to cause the anomalous current. In the

absence of M_y, the system has the symmetry $\sigma_y R_y \mathcal{T}$, leading to the disappearance of the anomalous current. Thus the anomalous current disappears for the Néel-type domain wall, and it reaches the maximum value for the Bloch-type domain wall. Also, the phase shift of anomalous Josephson junction oscillates in a sinusoidal relation to the azimuth angle φ_{az}, where the maximum value locates at $\varphi_{az} = \pi/2$. Several factors affecting the maximum phase shift as well as the amplitude of supercurrent are studied in detail.

For experiments, the QAHI-based anomalous Josephson junction can be connected with a normal 0 junction to construct a superconducting quantum interference ring. Varying the magnetic flux through the superconducting ring derives the current-phase relation presenting the existence of anomalous Josephson effect. For more significant effect, experimentalists can increase the magnetization, thicken the domain wall, and widen the junction. Also, by introducing a bare QAHI region, the phase shift could reach and exceed π, so it is possible to continuously drive the 0 junction into the π junction by changing the configuration of the domain wall or the magnetization strength. Consequently, this experimentally friendly anomalous Josephson junction could pave ways for realizing the potential phase battery as well as the superconducting quantum computation.

Acknowledgment

Qing Yan thanks Zhe Hou for helpful discussion.

References

[1] Josephson B 1962 *Phys. Lett.* **1** 251
[2] Anderson P W and Rowell J M 1963 *Phys. Rev. Lett.* **10** 230
[3] Makhlin Y, Schön G and Shnirman A 2001 *Rev. Mod. Phys.* **73** 357
[4] Xu W Z, Qin L X, Ye X G, Lin Fang, Yu D P and Liao Z M 2020 *Chin. Phys. B* **29** 057502
[5] Golubov A A, Kupriyanov M Y and Il'ichev E 2004 *Rev. Mod. Phys.* **76** 411
[6] Bulaevskii L N, Kuzii V V and Sobyanin A A 1977 *JETP Lett.* **25** 290
[7] Ryazanov V V, Veretennikov A V, Oboznov V A, Rusanov A Y, Larkin V A, Golubov A A and Aarts J 2000 *Physica C* **341–348** 1613
[8] Ryazanov V V, Oboznov V A, Rusanov A Y, Veretennikov A V, Golubov A A and Aarts J 2001 *Phys. Rev. Lett.* **86** 2427
[9] Zhu Y, Li W, Lin T H and Sun Q F 2002 *Phys. Rev. B* **66** 134507
[10] Zeng W and Shen R 2018 *Chin. Phys. B* **27** 097401
[11] Cheng Q and Sun Q F 2019 *Phys. Rev. B* **99** 184507
[12] Krive I V, Gorelik L Y, Shekhter R I and Jonson M 2004 *Low Temp. Phys.* **30** 398
[13] Krive I V, Kadigrobov A M, Shekhter R I and Jonson M 2005 *Phys. Rev. B* **71** 214516
[14] Buzdin A 2008 *Phys. Rev. Lett.* **101** 107005
[15] Reynoso A A, Usaj G, Balseiro C A, Feinberg D and Avignon M 2008 *Phys. Rev. Lett.* **101** 107001
[16] Szombati D B, Nadj-Perge S, Car D, Plissard S R, Bakkers E P A M and Kouwenhoven L P 2016 *Nat. Phys.* **12** 568
[17] Pal S and Benjamin C 2019 *Europhys. Lett.* **126** 57002
[18] Yokoyama T, Eto M and Nazarov Y V 2013 *J. Phys. Soc. Jpn.* **82** 054703
[19] Yokoyama T, Eto M and Nazarov Y V 2014 *Phys. Rev. B* **89** 195407
[20] Nesterov K N, Houzet M and Meyer J S 2016 *Phys. Rev. B* **93** 174502
[21] Zazunov A, Egger R, Jonckheere T and Martin T 2009 *Phys. Rev. Lett.* **103** 147004
[22] Cheng S G, Xing Y X, Xie X C and Sun Q F 2009 *Eur. Phys. J. B* **67** 551
[23] Brunetti A, Zazunov A, Kundu A and Egger R 2013 *Phys. Rev. B* **88** 144515
[24] Liu J F and Chan K S 2010 *Phys. Rev. B* **82** 125305
[25] Dolcini F, Houzet M and Meyer J S 2015 *Phys. Rev. B* **92** 035428
[26] Sakurai K, Ikegaya S and Asano Y 2017 *Phys. Rev. B* **96** 224514
[27] Minutillo M, Giuliano D, Lucignano P, Tagliacozzo A and Campagnano G 2018 *Phys. Rev. B* **98** 144510
[28] Liu J F and Chan K S 2010 *Phys. Rev. B* **82** 184533
[29] Ouassou J A and Linder J 2019 *Phys. Rev. B* **99** 214513
[30] Silaev M A, Tokatly I V and Bergeret F S 2017 *Phys. Rev. B* **95** 184508
[31] Assouline A, Feuillet-Palma C, Bergeal N *et al.* 2019 *Nat. Commun.* **10** 126
[32] Qi X L and Zhang S C 2011 *Rev. Mod. Phys.* **83** 1057
[33] Liu C X, Zhang S C and Qi X L 2016 *Annu. Rev. Condens. Matter Phys.* **7** 301
[34] Tokura Y, Yasuda K and Tsukazaki A 2019 *Nat. Rev. Phys.* **1** 126
[35] Chang C Z, Liu M H, Zhang Z C, Wang Y Y, He K and Xue Q K 2016 *Sci. Chin.-Phys. Mech. Astron.* **59** 637501
[36] He K, Ma X C, Chen X, Lü L, Wang Y Y and Xue Q K 2013 *Chin. Phys. B* **22** 067305
[37] Yu R, Zhang W, Zhang H J, Zhang S C, Dai X and Fang Z 2010 *Science* **329** 61
[38] Chang C Z, Zhang J S, Feng X *et al.* 2013 *Science* **340** 167
[39] Dziom V, Shuvaev A, Pimenov A *et al.* 2017 *Nat. Commun.* **8** 15197
[40] Xiao D, Jiang J, Shin J H *et al.* 2018 *Phys. Rev. Lett.* **120** 056801
[41] Chen B, Fei F C, Zhang D Q *et al.* 2019 *Nat. Commun.* **10** 4469
[42] Kou X F, Guo S T, Fan Y B *et al.* 2014 *Phys. Rev. Lett.* **113** 137201
[43] Chang C Z, Zhao W W, Kim D Y, Zhang H J, Assaf B A, Heiman D, Zhang S C, Liu C X, Chan M H M and Moodera J S 2015 *Nat. Mater.* **14** 473
[44] Sun H H and Jia J F 2017 *Sci. Chin.-Phys. Mech. Astron.* **60** 057401
[45] Li J H, Li Y, Du S Q, Wang Z, Gu B L, Zhang S C, He K, Duan W H and Xu Y 2019 *Sci. Adv.* **5** eaaw5685
[46] Gong Y, Guo J W, Li J H *et al.* 2019 *Chin. Phys. Lett.* **36** 076801
[47] Deng Y J, Yu Y J, Shi M Z, Guo Z X, Xu Z H, Wang J, Chen X H and Zhang Y B 2020 *Science* **367** 895
[48] Hubert A and Schäfer R 2009 *Magnetic Domains: The Analysis of Magnetic Microstructures* 2nd edn (Berlin: Springer) p. 201
[49] Spaldin N A 2010 *Magnetic Materials: Fundamentals and Applications* 2nd edn (Cambridge: Cambridge University Press) p. 85
[50] Li Z D, Hu Y C, He P B and Sun L L 2018 *Chin. Phys. B* **27** 077505
[51] Liu L, Chen W X, Wang R Q and Hu L B 2018 *Chin. Phys. B* **27** 047201
[52] Chen G, Ma T P, N′Diaye A T, Kwon H, Won C Y, Wu Y Z and Schmid A K 2013 *Nat. Commun.* **4** 2671
[53] Landau L and Lifshitz E 1935 *Phys. Z. Sowjetunion* **8** 153
[54] Chen G, Zhu J, Quesada A *et al.* 2013 *Phys. Rev. Lett.* **110** 177204
[55] Yasuda K, Mogi M, Yoshimi R, Tsukazaki A, Takahashi K S, Kawasaki M, Kagawa F and Tokura Y 2017 *Science* **358** 1311
[56] Wang J, Zhou Q, Lian B and Zhang S C 2015 *Phys. Rev. B* **92** 064520
[57] Zhou Y F, Hou Z, Lv P, Xie X C and Sun Q F 2018 *Sci. Chin.-Phys. Mech. Astron.* **61** 127811
[58] Zheng H and Jia J F 2019 *Chin. Phys. B* **28** 067403
[59] Yan Q, Zhou Y F and Sun Q F 2019 *Phys. Rev. B* **100** 235407
[60] Ding Y, Shen J, Pang Y, Liu G T, Fan J, Ji Z Q, Yang C L and Lü L 2013 *Acta Phys. Sin.* **62** 167401 (in Chinese)
[61] Li C A, Li J and Shen S Q 2019 *Phys. Rev. B* **99** 100504(R)
[62] Zhou Y F, Hou Z and Sun Q F 2018 *Phys. Rev. B* **98** 165433
[63] Datta S 1995 *Electronic Transport in Mesoscopic Systems* (Cambridge: Cambridge University Press) pp. 141–151
[64] Qi X L, Hughes T L and Zhang S C 2010 *Phys. Rev. B* **82** 184516
[65] Likharev K K 1979 *Rev. Mod. Phys.* **51** 101
[66] Anderson P W and Dayem A H 1964 *Phys. Rev. Lett.* **13** 195
[67] Baratoff A, Blackburnf J A and Schwartzf B B 1970 *Phys. Rev. Lett.* **25** 1096
[68] Gregers-Hansen P E, Levinsen M T and Pedersen G F 1972 *J. Low Temp. Phys.* **7** 99
[69] Sun Q F, Wang J and Lin T H 1999 *Phys. Rev. B* **59** 3831
[70] Sun Q F, Wang B G, Wang J and Lin T H 2000 *Phys. Rev. B* **61** 4754
[71] Sun Q F, Guo H and Wang J 2002 *Phys. Rev. B* **65** 075315
[72] Li Y H, Liu J, Song J T, Jiang H, Sun Q F and Xie X C 2018 *Sci. Chin.-Phys. Mech. Astron.* **61** 97411
[73] Cuevas J C, Martín-Rodero A and Yeyati A L 1996 *Phys. Rev. B* **54** 7366
[74] Dresselhaus M S, Dresselhaus G and Jorio A 2008 *Group Theory: Application to the Physics of Condensed Matter* (Berlin: Springer) p. 403
[75] Ji Y Q, Niu Z P, Feng C D and Xing D Y 2008 *Chin. Phys. Lett.* **25** 691
[76] Clarke J and Pippard A B 1969 *Proc. R. Soc. Lond. A* **308** 447